# A Numerical Analysis of Different Micro-Textures in Improving Tribological Properties of Surfaces

Roland Bejjani * and Marc Chamoun

Department of Industrial and Mechanical Engineering, School of Engineering, Lebanese American University, Byblos, Lebanon
Email: rolandbejj@gmail.com (R.B.); marcchamoun1@outlook.com (M.C.)

***Abstract*—Laser surface texturing has become an important technology to improve the tribological properties of surfaces under lubricated friction. While several studies have analyzed how different micro-textures affect hydrodynamic pressure generation, further study of how distinct characteristics of the micro-texture geometry affect pressure generation remains needed. This study aims at conducting a comparative analysis of an optimized and modified chevron micro-texture with other conventional micro-textures used in literature using computational fluid dynamic simulations. The study showed that the modified chevron micro-texture with a large leg-width ratio outperformed other conventional micro-texture shapes such as the circle and rectangle by generating an asymmetric pressure distribution. Notably, the modified chevron configuration achieved a hydrodynamic pressure build-up approximately 44.1% greater than the rectangle geometry and 100.8% greater than that of the circular geometry. The experimental analysis conducted confirms the modified chevron micro-texture's expected frictional performance observed in the Computational Fluid Dynamic (CFD) simulations, where the modified chevron decreased the friction coefficient by 9.25% compared to the untextured case. The results of this study can be significant for various sliding applications in the automotive and aerospace industries.**

***Keywords*—micro-texture, computational fluid dynamics, friction reduction, pressure build-up**

## I. Introduction

Micro-textured surfaces have become a notable method used to improve the tribological properties of surfaces by reducing friction and wear under various contact conditions. With the adoption of various methods to engrave micro-textures on different surfaces, Laser Surface Texturing (LST) demonstrated various advantages over other technologies which includes its high versatility, accuracy, and stability [1]. Laser beams are made out of light particles called photons, which, when directed towards a surface inside a focus and minuscule area, will initiate a process called laser ablation [2]. Laser ablation consists of a transfer of energy occurring between the incoming high-energy laser photons with the electrons present on the surface of the targeted workpiece. The high-energy transfer will excite the electrons on the surface, which will generate heat, removing the material at the micro-scale by melting followed by vaporization of the material [2]. The laser ablation phenomenon is dependent on Beer Lambert's Law, which states that the quantity of light absorbed by the material is affected by the thickness of the material as well as by the intensity of the light source [2].

An important parameter of LST is the pulse duration of the laser. Laser machines used in literature to engrave micro-textures on surfaces can be characterized into long-pulsed lasers and ultra-short, pulsed lasers. The duration of a single laser pulse heavily affects the quality of the engraved micro-textures, for example, a pulse duration greater than a few picoseconds can lead to Heat-Affected Zones (HAZ) on the surface, because the electrons transfer energy to the lattice on nanoseconds timescales, raising the material's temperature. This can lead to the formation of molten material around holes engraved on surfaces using a nanosecond laser, decreasing the surface quality of the textures, however, when using an ultra-short pulsed laser, such as the femtosecond laser, the formation of molten material and HAZs around the micro-textures was avoided [3]. In such a case, there is not enough time for the transfer of energy from the electrons to the lattice to take place, leading to the engravement of more precise micro-textures with improved surface roughness and properties.

## II. Literature Review

Laser-induced micro-textures can play a vital role in enhancing the tribological properties of surfaces, with different friction mechanisms depending on the state of the contact conditions. Under dry friction conditions, micro-textures can decrease friction by reducing the contact area and trapping wear debris, while under lubricated friction, micro-textures play the role of secondary lubricant reservoirs, at the same time increasing

Manuscript received September 23, 2026; revised October 29, 2026; accepted March 11, 2026; published May 13, 2026.

doi: 10.18178/ijmerr.15.3.248-259

the load-carrying capacity of the fluid, due to the generation of hydrodynamic pressure inside the lubricant, reducing the friction coefficient [1]. Surface micro-textures can be applied in various applications in order to improve the tribological and mechanical properties of surfaces, such as cylinder-liner piston rings [4], journal bearings [5], cutting tools [6], and mechanical seals [7]. In order to study how micro-textures can generate hydrodynamic pressure under lubricated contact, current research has utilized Computational Fluid Dynamic (CFD) numerical analysis by simulating hydrodynamic lubricated friction between two a micro-textured and an untextured surface, which also involves the process of understanding the effects of the geometrical parameters of the texture on hydrodynamic pressure generation, while also aiming at optimizing these parameters for better experimental friction reduction performance through the use of tribometers.

### *A. Non-Converging Textures*

A notable micro-texture studied extensively in literature is the circular micro-texture, where CFD hydrodynamic simulations found that increasing the texture's depth from 25 μm to 35 μm enhanced the load-carrying capacity of the fluid, consequently decreasing the friction coefficient [8]. It was noted that increasing the depth, up to a certain limit, is beneficial, since a big enough micro-texture depth could prompt the formation of micro-vortex regions, which consume kinetic energy coming from the sliding upper surface, decreasing the amount of energy available to generate hydrodynamic pressure, leading to a decrease in the load-carrying capacity [8]. Two-dimensional fluid simulations on a cylindrically shaped micro-texture demonstrated that increasing the texture's depth beyond a certain threshold will also enhance micro-vortex formation inside the texture, which is detrimental to the lubricant's load carrying capacity [9]. Ring-on-ring numerical simulations employing a variety of micro-textures such as circular textures, linear and wavy grooves showed that these micro-textures can act as secondary lubricant reservoirs under mixed or boundary lubrication regimes, while also increase the pressure of the lubricant due to the squeezing effect of the lubricant by the converging-wedge, inertial flow effects, and cavitation, which collectively enhanced the load-carrying capacity of the fluid [10]. Sector-shaped textures, obtained by cutting a circular dimple into a circular sector using two intersection chord lines, were tested using CFD simulations, where it was shown that such a shape can generate more hydrodynamic pressure compared to the regular circular, rectangle and triangle textures, leading to a pin-on-disk friction reduction test of 60% compared to the circular texture [11]. Another significant parameter is the area density of the micro-textures, where an increase in the area density of circular micro-textures from 3% to 50% increased the lift coefficient by 2272.5%, which indicates an increase in the load-carrying capacity of the lubricant [8].

### *B. Converging Textures*

Micro-textures with a converging geometry such as the triangle and chevron or V-shaped micro-texture have also been extensively studied for their friction reduction abilities. For example, the triangular texture engraved on stainless steel specimens outperformed the circular texture under lubricated ball-on-ring friction tests due to its increased ability in generating hydrodynamic lift and thus reducing friction [12]. A numerical fluid simulation study revealed that the chevron micro-texture, due to its converging geometrical shape, is able to form an asymmetric pressure distribution which gives the lubricant a load-carrying capacity, separating the two surfaces away from each other, reducing friction [13]. The influence of the chevron's geometrical parameters such as the depth, leg width, leg length, opening angle, as well as the arrangement and area density, on the load-carrying capacity of the fluid was investigated. For example, an increase in the depth of the chevron texture from 17% to 167% of the film's thickness increased the load-carrying capacity, with the optimal value of the depth equal to the lubricant film's thickness [14]. When increasing the leg width of the chevron, the outflow at the converging wedge of the chevron increased, enhancing the generated pressure inside the lubricant. The chevron micro-texture outperformed other textures such as well such the triangular texture by a better increase in load-carrying capacity [15]. The scale of the chevron micro-texture is also an important factor, as small-scaled chevrons with a leg width of 5 μm decreased friction by 89%, while large scale chevron with a leg width range of 200–400 μm led to no noticeable friction reduction [16]. The chevron's geometrical characteristics of two converging legs offer greater hydrodynamic pressure generation and load-carrying capacity when the chevron texture is directed along the sliding direction, outpacing non-converging textures such as circular and linear grooves [17]. Other converging-shaped textures were also shown to outperform non-converging ones, such as a kite-shaped texture, which was shown to generate higher hydrodynamic pressure values than the circle, square, and triangular textures at an area density of 30% [18].

### *C. Bio-Inspired Textures*

Several studies have analyzed micro-textures inspired by geometries found in nature. For example, a study [19] of micro-texture inspired by the body shape of a falcon bird was evaluated using CFD numerical simulations; acute and converging wedge-shaped outlets were found to be more effective at directing the lubricant's flow and promoting lubricant accumulation compared to texture with a linear outlet. Furthermore, the leading edge geometry expanded the regions of negative pressure and cavitation, thereby decreasing the real contact area between the surfaces. A fluid numerical simulation was carried on a parabolic, fish skin-inspired micro-texture, where it was noted that increasing the parabolic length-to-width ratio, which essentially elongates the parabolic texture laterally, decreased the hydrodynamic pressure generated since a stretched-out geometry weakened the converging-effect [20]. Another study [21] on bio-inspired teardrop micro-texture demonstrated increases in the load-carrying capacity by 45%, 43%, and 30% compared to circular, square, and elliptical

micro-textures, respectively. It was also noted that beyond an area density of 29%, no significant gains in hydrodynamic pressure generated was observed, agreeing with the current literature reporting an optimal area density of 20–40%.

As previously mentioned, the chevron micro-texture, due to its geometrical converging shape, demonstrates improved friction reduction performance compared to other textures. The chevron micro-texture could be further improved by better understanding how its geometrical parameters affect hydrodynamic pressure, while proposing a new geometrical modification to enhance its hydrodynamic pressure generation performance. The purpose of the present study is to better understand how the different geometrical parameters of the chevron micro-texture affect hydrodynamic pressure build-up, including its depth, leg length, opening angle, and a newly defined parameter, the leg width ratio. While a univariate analysis does not capture the interaction effects between the different parameters, it can be useful to understand the individual effect of varying each geometrical parameter on the friction performance. Moreover, the study aims to perform a comparative analysis between the modified chevron with the circular and rectangular micro-textures on their hydrodynamic pressure generation to better understand the effect of the shape of the texture on the fluid behavior difference. The fluid behavior inside the micro-textures, as well as the hydrodynamic pressure generated will be investigated. The friction performance of the modified chevron texture will be validated experimentally. These results can be beneficial through the application of the chevron micro-texture in several real-life applications to decrease friction such as hydrodynamic journal bearings [5], hydraulic components such as pumps and valves [22], and cutting tools [6, 23].

## III. Materials and Methods

### A. Governing Fluid Equations

Computational fluid dynamic simulations were performed using the Ansys Fluent in Ansys 2024 R2. The governing fluid equations include the Navier-Stocks momentum and continuity equations, expressed in vector form as per Eqs. (1) and (2), respectively:

$$\rho(\vec{u}.\nabla)\vec{u} = -\nabla p + \nabla \cdot (\mu \nabla \vec{u}) \quad (1)$$

$$\nabla \cdot \vec{u} = 0 \quad (2)$$

where $\rho$ is the lubricant density, $\vec{u}$ is the velocity vector, along with its velocity components, $u$, $v$, and $w$ in the x, y, and z directions, respectively, $p$ is the static pressure and $\mu$ is the lubricant's dynamic viscosity.

The parameters that will be used to determine the tribological performance of the different micro-textures will include the hydrodynamic friction coefficient and the average static pressure build-up at the upper sliding surface of the friction pair, which is directly proportional to the load-carrying capacity force.

The load carrying capacity force $F_y$ and the friction force $F_z$ are calculated as per Eqs. (3) and (4), respectively:

$$F_y = \iint p(x,z)dxdz \quad (3)$$

$$F_z = \iint \tau(x,z)dxdz \quad (4)$$

where $p(x,z)$ and $\tau(x,z)$ are the pressure and shear stress at position $(x,z)$ on the surface of the lubricant, respectively. Thus, the "hydrodynamic" coefficient of friction can be calculated as per Eq. (5):

$$COF = \frac{F_z}{F_y} \quad (5)$$

The defined friction coefficient $f$ differs from the conventional friction coefficient used in mechanics which is defined as the applied normal force over the friction force. In this case, $f$ represents a "hydrodynamic" friction coefficient, used by various other studies in the Refs [8, 14], which is defined as the load-carrying capacity lift force, acting on the upper sliding surface, and generated inside the lubricant by the micro-texture, over the friction force acting on that same surface. This friction coefficient is used to measure the hydrodynamic efficiency of a micro-texture, where a low friction coefficient indicates a large load-carrying capacity force with a low friction force [24]. The pressure build-up as well as the friction coefficient are calculated at the upper sliding surface of the domain.

### B. Simulation Process

#### 1) Simulated friction model and boundary conditions

The fluid domain shown Fig. 1 was designed using SolidWorks 2023 to be imported into Ansys Workbench 2024 R2. The inlet and outlet boundary conditions of the domain are considered as periodic boundaries, which simulates the repetition of the domain, while the lateral boundary conditions are set to be symmetric.

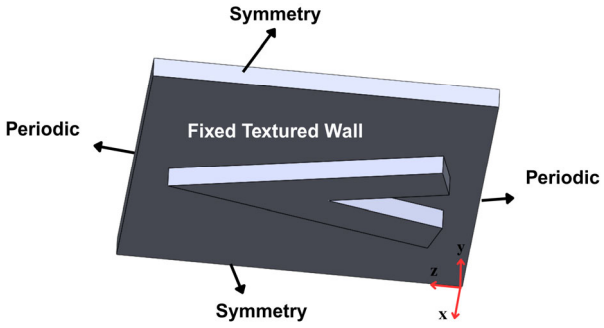


Fig. 1. Fluid domain.

The bottom textured surface of the domain is a fixed wall, while the upper untextured sliding surface is sliding in the z-direction at a fixed speed U equal to 1 m/s, as shown in Fig. 2. The lubricant's film thickness H will be

set to 30 µm, while d is the depth of the micro-texture in µm as well, as portrayed in Fig. 2.

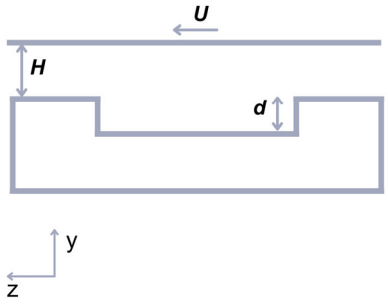


Fig. 2. Simulated friction model.

*2) Lubricant properties*

The lubricant was modeled as a single-phase, incompressible fluid. The flow was solved in steady state, without physical time integration. The lubricant properties were set to the following, matching a low viscosity mineral oil fluid:

- Density: $\rho = 853$ kg/m$^3$;
- Dynamic viscosity: $\mu = 0.0027$ Pa.s.

*3) Texture geometry definitions and parameter variations*

The geometrical parameters of the chevron or V-shaped texture are shown in Fig. 3, where l is the length of the chevron's leg, $\alpha$ is the opening angle, $w_1$ and $w_2$ are the initial and final width of the chevron's leg, forming the leg width ratio parameter $w_r$ defined as per Eq. (6):

$$w_r = w_2/w_1 \tag{6}$$

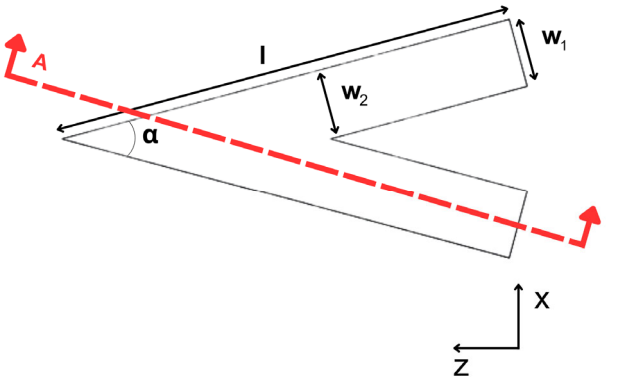


Fig. 3. Geometrical parameters of the chevron micro-texture.

The ranges and baselines "fixed" values of the chevron geometrical parameters are summarized in Table I. In the analysis of the parameters, a single parameter was varied at a time while the remaining parameters were held at their fixed values, allowing the influence of each geometrical parameters on the hydrodynamic fluid behavior to be assessed independently.

TABLE I. SUMMARY OF THE CHEVRON PARAMETER VARIATIONS WITH THE FIXED VALUES

| Parameter | Variation 1 | Variation 2 | Variation 3 | Fixed Value |
|---|---|---|---|---|
| Depth (d-µm) | 15 | 30 | 60 | 30 |
| Angle (α-deg) | 30 | 60 | - | 30 |
| Length (l-µm) | 300 | 400 | 500 | 400 |
| Leg width ratio ($w_r$) | 0.36 | 1 | 1.25 | 1 |
| [$w_2/w_1$] | [37.77/60] | [60/60] | [75.29/60] | [60/60] |

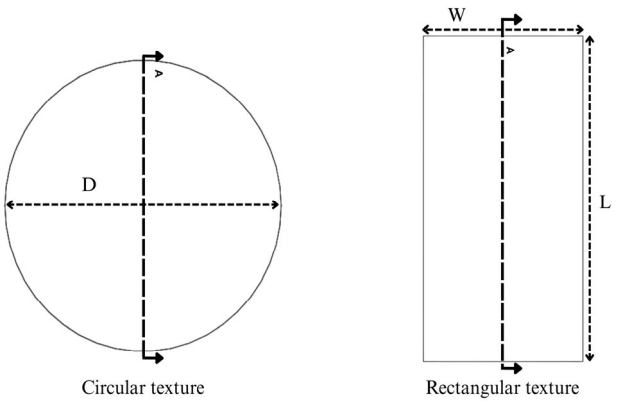


Fig. 4. Geometrical parameters of the circular and rectangular micro-textures.

As previously mentioned, the proposed chevron micro-texture will be compared with the friction reduction performance of the circular texture and the rectangular textures of similar scale and size. The diameter of the circular texture D will be fixed at 414 µm, while the length L and width W of the rectangular micro-texture will be set to 402 µm and 207 µm, respectively, as shown in Fig. 4. The depth of both micro-textures is fixed at 30 µm as well.

The geometrical parameters of the rectangular and circular textures were chosen so that these textures would occupy the same space when engraved on a surface. This can be visualized in Fig. 5, where it can be observed that the three micro-textures that will be compared will occupy the same space, ensuring a valid comparison.

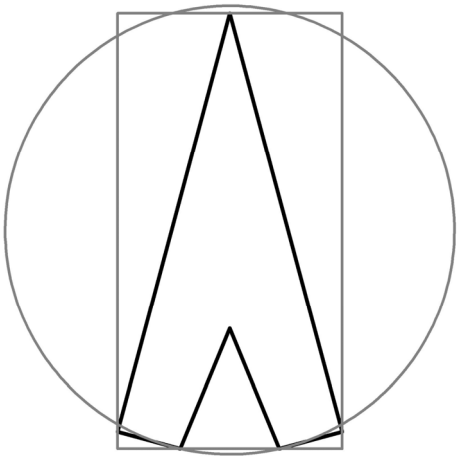

Fig. 5. Superposition of the micro-texture shapes.

*4) Meshing procedure*

The computational fluid domain was discretized with hex8 elements, as shown in Fig. 6. The mesh is finer inside of the micro-texture volume, where Cell size 1 represents the cell size of the lubricant film volume, while Cell size 2 represents the cell size of the micro-texture volume.

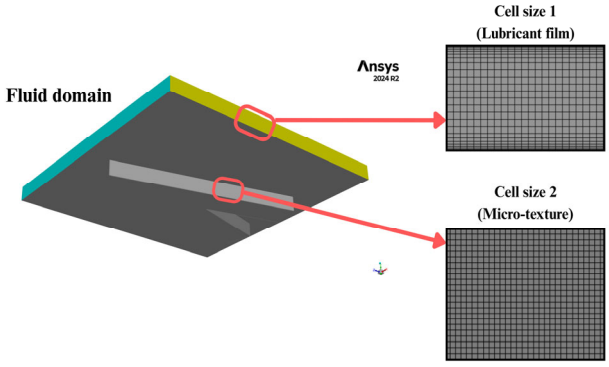


Fig. 6. Mesh grid.

In order to ensure that the mesh used is independent from further refinement, a mesh independence study was conducted using the Grid Convergence Index (GCI) method, for both of the hydrodynamic Coefficient of Friction (COF) and the pressure build-up. Table II shows the results of the mesh independence study. The mesh cell refinement ratio is equal to 1.5 for both cell sizes.

TABLE II. MESHING RESULTS

| Mesh | Cell size 1 (µm) | Cell size 2 (µm) | Pressure Build-Up (Pa) | COF |
|---|---|---|---|---|
| Coarse | 4.5 | 3 | 37.29 | 2.356 |
| Medium | 3 | 2 | 38.637 | 2.271 |
| Fine | 2 | 1.3333 | 38.907 | 2.255 |

TABLE III. GCI RESULTS FOR THE PRESSURE BUILD-UP

| GCI Results | Value |
|---|---|
| Order of accuracy | 3.96 |
| Refinement ratio | 1.5 |
| Finest mesh error | 0.0676 |
| Safety Factor (Fs) | 1.25 |
| GCI | 0.0846 |
| GCI (%) | 0.217 |

The GCI results for the pressure build-up, shown in Table III, indicate a positive order of accuracy value and thus a converging mesh with refinement. The finest mesh error can be estimated to be equal to 0.0676. Taking into consideration a safety factor of 1.25, the GCI (%), which also represents the discretization error, is thus equal to 0.217%. Therefore, the reported results for the pressure build-up are considered grid-independent within the stated numerical uncertainty.

A similar procedure was conducted for the COF, as shown in Table IV, to ensure that the grid is independent from further refinement for the tribological properties used to measure performance. The order of accuracy is positive as well, with a final GCI (%) equal to 0.191%.

Inflation layers are placed on the upper moving wall and the bottom textured walls.

TABLE IV. GCI RESULTS FOR THE COF

| GCI Results | Value |
|---|---|
| Order of accuracy | 4.18 |
| Refinement ratio | 1.5 |
| Finest mesh error | –0.00347 |
| Safety Factor (Fs) | 1.25 |
| GCI | 0.00433 |
| GCI (%) | 0.191 |

*5) Solver settings*

The simulations were solved in ANSYS Fluent using a pressure-based steady-state formulation with a coupled pressure-velocity scheme. PRESTO! (PREssure STaggeting Option) scheme was used for the pressure interpolation, which computes face pressure using a staggered-control-volume formulation based on discrete continuity. This choice is compatible with periodic domains and was adopted to improve the accuracy of pressure interpolation in the presence of localized pressure gradients induced by the micro-texture geometry. Second-order upwind was used for the momentum discretization. The residuals for the continuity were set at 1e−3, while the velocity residuals in the x, y, and z directions were set at 1e−6. Since the solution was steady state, no physical time step was set. The under-relaxation parameters for the pressure, momentum, and density were set to 0.5, 0.5, and 1, respectively. The required number of iterations was around 100 iterations.

The flow was set to laminar. It is important to note that any negative pressure values observed in the simulation results do not indicate pressures below the vapor pressure or vacuum conditions. The minimum absolute pressure within the fluid domain is 100.7 kPa, while the vapor pressure of the lubricant is 0.66 kPa. Therefore, cavitation conditions are not reached, and the implementation of a cavitation model was not necessary to capture the overall trends. This approach is consistent with previous studies reported in the literature, where a cavitation model was also deemed unnecessary for observing general trends [25, 26].

*C. Lazer Texturing Process*

A femtosecond laser machine will be used to engrave the modified chevron micro-texture on the surface. The laser parameters such as frequency, power, jumping speed, jumping delay, marking speed, laser path, and gap distance between hatch lines all affect the quality of the micro-textures and thus should be optimized. For example, a large hatch distance of 10 µm made it so that the engraved lines are visible, which means that the texture was not engraved well, while a smaller hatch distance of 2 µm is more suitable, as shown in Fig. 7.

Ongoing research is taking place to validate the friction performance results of the proposed chevron micro-texture using a tribometer. The present research will provide key

insights into effective micro-texture design in the aim of improving the friction performance of the texture by generating hydrodynamic pressure. This understanding will be used in order to better propose novel micro-texture designs that can further decrease friction under lubricated contact compared to other conventional textures used in current literature.

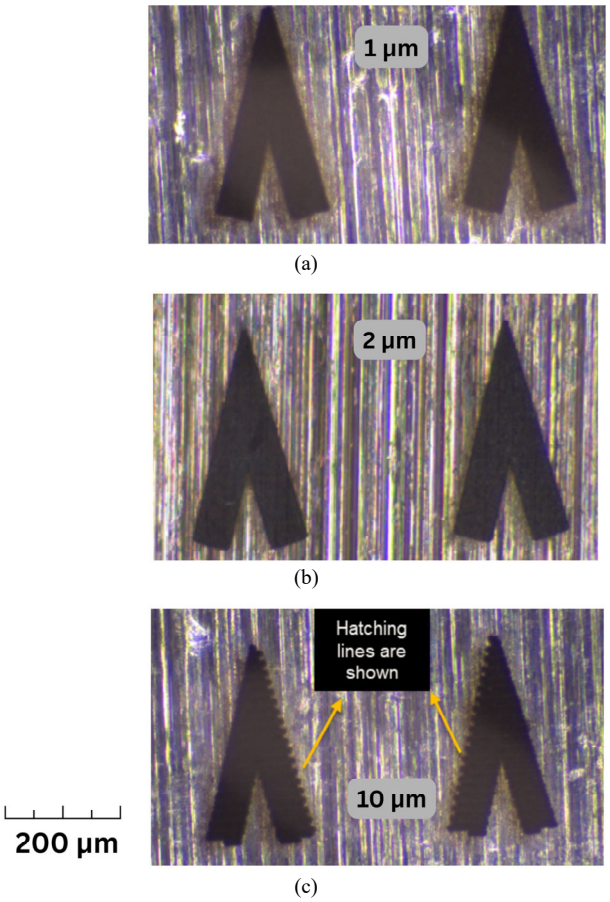


Fig 7. Effect of the gap distance between hatching lines on the chevron micro-texture, with gap distances of (a) 1 µm; (b) 2 µm; and (c) 10 µm.

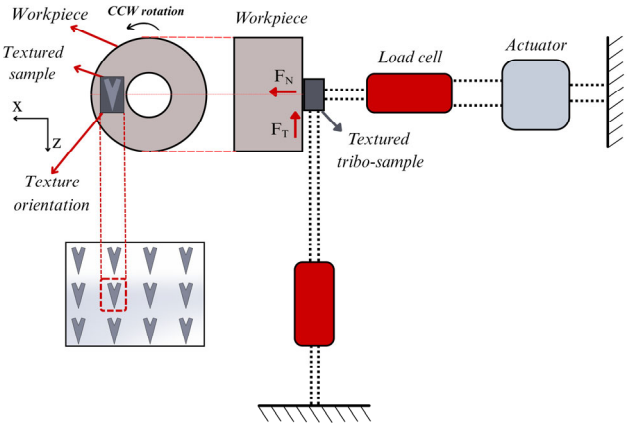


Fig. 8. Experimental setup.

### D. Experimental Setup and Materials

The experimental setup used was developed in prior work [27]. P25-grade carbide samples were engraved using laser surface texturing, while the workpiece is made of ST-37 steel, which was cut using waterjet cutting into a ring shape, grinded using a horizontal surface grinder machine, and polished with #2000 abrasive paper. The detailed experimental setup, with front and side views, are shown in Fig. 8. The textured tribo-sample is fixed onto the tribometer, while the steel workpiece is mounted on a Siemens Sinumerik 808D CNC lathe. The steel workpiece is rotating in the counterclockwise direction, with the textured tribo-sample oriented downwards, which is along the sliding direction. The normal $F_N$ and tangential force $F_T$ are monitored using two separate load cells. The experimental friction coefficient was calculated by dividing the average tangential force over the average normal force, as shown in Eq. (7):

$$\mu = \overline{F_T} \Big/ \overline{F_N} \tag{7}$$

It is relevant to note that the setup was modified in order to test the micro-textures under surface-to-surface contact. This was conducted by using the frontal annular face of a ring-shaped workpiece as the contact interface, instead of using the curved circumferential surface of a solid cylindrical bar. The lubricant used for experiments is mineral oil.

## IV. Result and Discussion

### A. Effect of Chevron Opening Angle

The opening angle of the chevron micro-texture was shown to have a notable impact on the hydrodynamic pressure generated. The hydrodynamic pressure and COF results are shown in Fig. 9. The opening angle was set to a low value of 30º and a relatively high value of 60º. It can be seen from Fig. 9 that a small opening angle of 30º led to a pressure build-up of 33.42 Pa and a resulting friction coefficient of 2.63. Doubling the angle to 60º reduced the hydrodynamic pressure generated by a large margin, to a value of 3.30 Pa, along with a friction coefficient of 26.74. Such a drastic difference can be explained by analyzing the flow vectors in Fig. 10. In this case, the flow direction plays a key role. At a small angle of 30º, the flow does not deviate much from the general flow direction, however, at an opening angle of 60º, the flow deviates from the general flow direction, with the formation of significant micro-vortices inside the texture. This significant flow deviation, which results in micro-vortex formation, dissipates kinetic energy and decreases its availability to generate enough hydrodynamic pressure. Thus, the lesser the flow deviates from the general flow direction of the sliding surface, the more energy is available to build-up pressure inside the lubricant. This flow behavior affected by the increase in the chevron opening angle is also observed in current literature by Shen *et al.* [14], where it was demonstrated that small angles do not deviate the flow, while higher angles can lead to flow deviation and micro-vortex regions, which in turn consume kinetic energy and decreases hydrodynamic pressure.

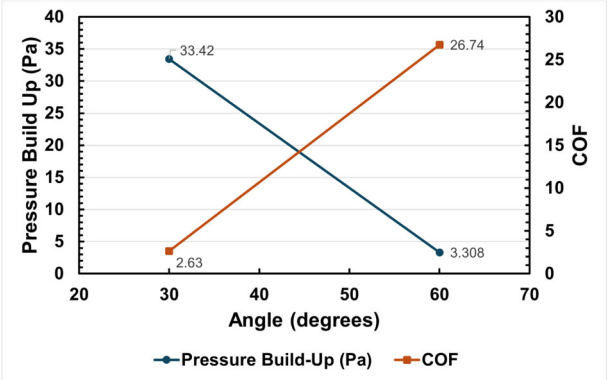


Fig. 9. Effect of opening angle of pressure build-up and COF.

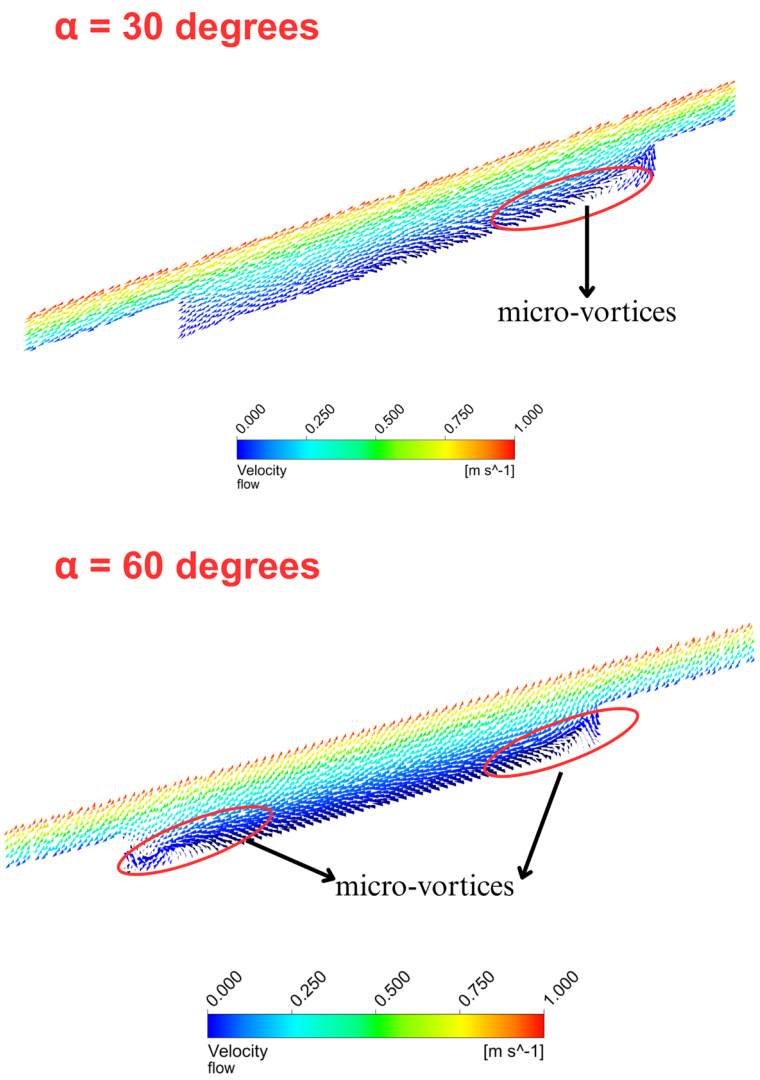


Fig. 10. Velocity vectors cross-section through section A at opening angles 30 and 60 degrees.

### *B. Effect of Chevron Depth*

The depth of the chevron micro-texture was also observed to affect greatly the hydrodynamic pressure build-up. The depth of the texture was changed three times. For a depth of 15 µm, the pressure build-up generated was 29.38 Pa, with a friction coefficient of 2.99, as shown in Fig. 11. Increasing the depth to 30 µm increased the pressure build-up to 33.42 Pa. However, further increasing the depth to a value of 60 µm significantly reduced the generated pressure to 27.24 Pa, with an increased friction coefficient value of 3.22. The velocity vectors for each depth are included in Fig. 12, where it can be seen that a low depth of 15 µm resulted in a small micro-vortex region at the inlet of the texture while the lubricant is entering the texture.

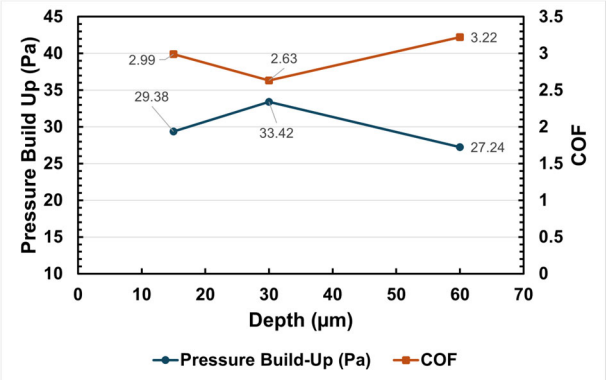


Fig. 11. Effect of depth on the pressure build-up and COF.

While increasing the depth of the chevron micro-texture to 30 μm increased the size of the micro-vortex region at the inlet of the texture, the pressure build-up has increased, that is because a low micro-texture depth does not let enough fluid to enter and exit the texture to generate enough hydrodynamic pressure build-up. At a depth of 60 μm, significant micro-vortex regions were formed throughout the texture, along with backflow at the bottom, which both consume kinetic energy, diminishing the generation of hydrodynamic pressure [9]. A depth of 30 μm, which is equal to the lubricant's film thickness, was found to be the most optimal in enhancing tribological performance, which is supported by current literature as well [9]. The fluid behavior, as well as the hydrodynamic pressure trend observed when the depth is increased is comparable to the results of Shen *et al.* [14], where as the depth of the chevron texture increased, more fluid can go into the texture, increasing the load-carrying capacity. However, as the depth continues to be increased from 30 μm to 50 μm, micro-vortex regions start to form, which consume kinetic energy and reduce the hydrodynamic pressure generation, followed by an increase in the COF by 15.38%. This aligns with the increase of the COF by 22.43% when the texture depth increased from 30 μm to 60 μm in this study.

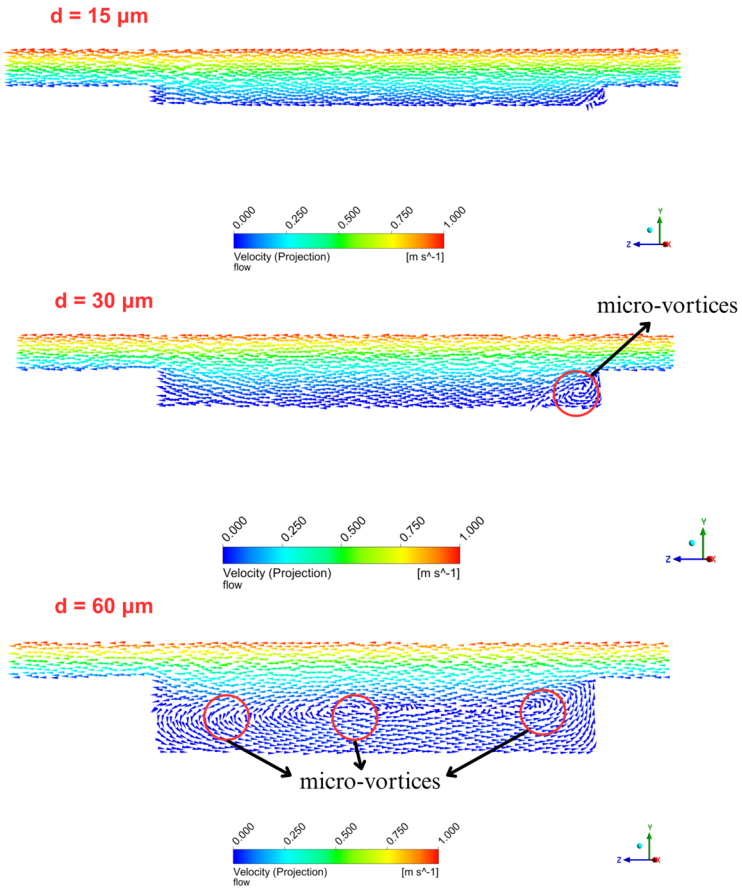


Fig. 12. Velocity vectors cross-section through section A at depths of 15, 30, and 60 μm.

## C. *Effect of Chevron Length*

The length of the chevron's leg is also an important parameters that affected the hydrodynamic pressure build-up of the fluid. At a length of 300 μm, the hydrodynamic pressure build-up generated at this length is 24.86 Pa, the lowest amongst the three, with a relatively high friction coefficient of 3.55, as shown in Fig. 13, leading to the highest. The velocity vectors cross-section shown in Fig. 14 showcases a notable micro-vortex region as the fluid is entering the texture at a length of 300 μm. Increasing the length of the chevron's leg to 500 μm decreased the micro-vortex region and thus led to a higher pressure build-up equal to 38.75 Pa, with the lowest friction coefficient amongst to the other lengths equal to 2.26. Literature mentions that a small chevron micro-texture length increased the micro-vortex formation,

which increased kinetic energy consumption and thus diminished the micro-texture's ability to generate hydrodynamic pressure build-up inside the lubricant, leading to a high COF [14]. The second length variation, which increased the leg length of the chevron from 400 µm to 500 µm, decreased the COF by 14.06%. Shen *et al.* [14] varied the chevron's leg length between around 400 µm and 500 µm as well, leading to a decrease in the COF by 16.36%, showing a similar trend, who noted that small chevron lengths led to significant micro-vortex regions compared to higher lengths, noting that increasing the length increased the load-carrying capacity and thus reduced the friction coefficient. The small percentage difference can be explained by inconsistent area densities, and thus periodic distances between the micro-textures.

Even though the highest leg lengths brought better results, increasing the length when the area density of the micro-texture on the surface remains unchanged does not increase the quantity of lubricant flowing inside the micro-texture [14]. Moreover, increasing the leg lengths with the rest of the geometrical parameters remaining unchanged would decrease the area density, negatively affecting the hydrodynamic pressure build-up inside the lubricant.

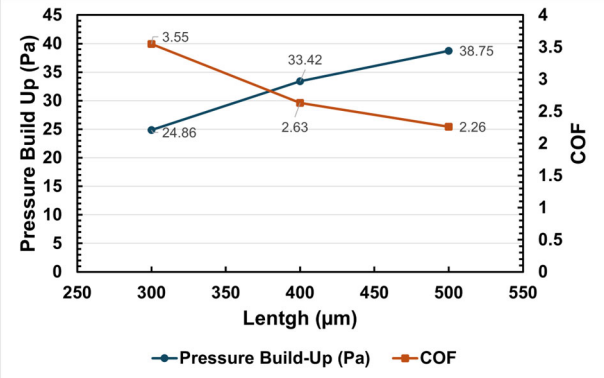


Fig. 13. Effect of chevron leg length on the pressure build-up and COF.

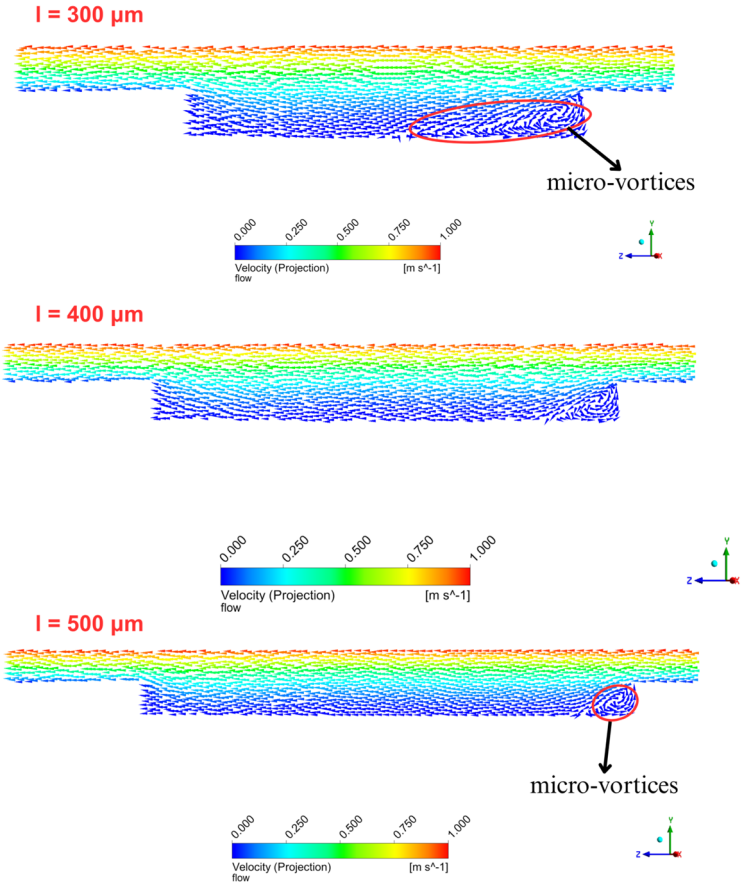


Fig. 14. Velocity vectors cross-section through section A with the leg lengths of 300, 400, and 500 µm.

## D. *Effect of Chevron Leg Width Ratio*

This parameter was proposed in order to study the effects of narrowing or enlarging the path of the lubricant inside the chevron's legs on the resultant hydrodynamic pressure build-up. The conventional micro-texture with a leg width ratio equal to 1 resulted in a hydrodynamic pressure build-up of 33.42 Pa, with a COF of 2.63, as shown in Fig. 15. Decreasing the leg width ratio to 0.36, which essentially narrows the lubricant's path inside the micro-texture, decreased the hydrodynamic pressure generated to 26.97 Pa, and thus increased the COF to a value of 3.28.

Based on the pressure curves in Fig. 16, while the chevron with a leg width ratio of 0.36 led to lower negative pressure values than the conventional chevron, the narrowed chevron had lower positive pressure build-up values than the conventional chevron. The narrow legs

reduced the area of the converging outlet in that case, which affected the pressure generated. Increasing the leg width ratio to 1.25 increased the hydrodynamic pressure to 38.9 Pa, outperforming the conventional chevron, with a lower COF of 2.25. A larger width ratio led to a larger outlet converging area, which led to higher pressure build-up values at the upper surface as shown in the pressure curves of Fig. 16.

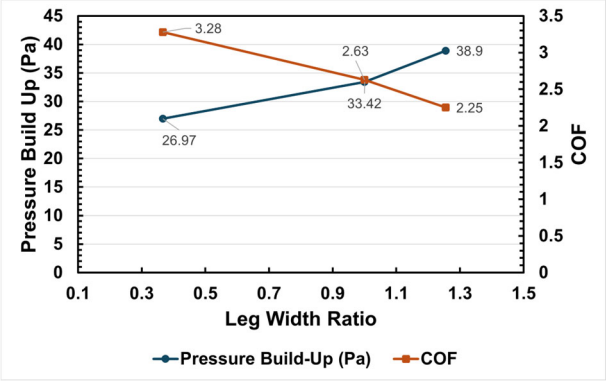


Fig. 15. Effect of chevron leg width ratio on pressure build-up and COF.

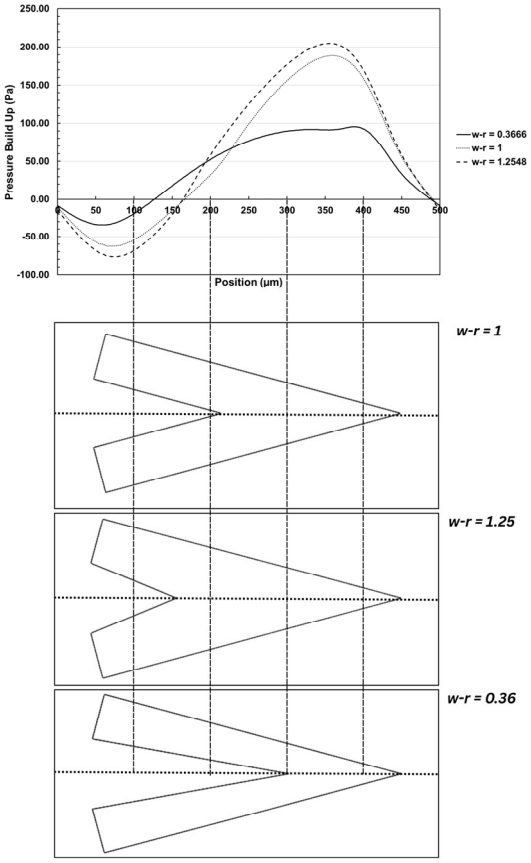


Fig. 16. Pressure build-up curve over the line coincident with section A on the upper sliding surface for the chevron micro-textures of leg width ratio equal to 1, 1.25 and 0.36.

Thus, it can be concluded that the outlet converging area of the texture, which is affected by the leg width ratio in this case, is a significant geometrical parameter in generating pressure. A smaller and narrowed down outlet area decreased the pressure build-up generated, since not enough lubricant flowed inside the texture, while a larger outlet area increased the amount of fluid going into the texture, which increased the hydrodynamic pressure generated. The modified chevron micro-texture with a higher leg width ratio thus provides better friction reduction performance compared to the conventional chevron.

The effects of the studied chevron parameters on the hydrodynamic COF are summarized in Table V.

TABLE V. SUMMARY OF THE PERCENTAGE CHANGES OF THE PARAMETER VARIATIONS

| Parameter | Angle | Depth | Length | Leg Width |
|---|---|---|---|---|
| 1st % COF Change | 917.7% | −12.04 | −25.9 | −19.81 |
| 2nd % COF Change | - | 22.43 | −14.06 | −14.44 |

## E. Micro-Texture Comparison Analysis

The modified chevron micro-texture with an increased leg width ratio was compared with other non-converging conventional micro-texture shapes such as the circular and rectangular micro-textures. Fig. 17 shows the pressure build-up curves at the upper sliding surface for each of the three different micro-textures. It can be noticed that both the circular and rectangular textures have higher peak values of positive pressure build-up. However, both achieved hydrodynamic pressure build-up values of 19.37 Pa for the circle and 27.00 Pa for the rectangle, both being lower than the pressure generated by the modified chevron, with higher COFs as well, as listed in Table VI. Even though the modified chevron had lower positive pressure peak values, the pressure distribution is more asymmetric, in favor of the positive area below the curve, than the other two textures. This means that the negative pressure area at the upper surface is much smaller in size and value than the positive pressure area, since the negative area below the curve is smaller than the positive pressure area. The pressure distribution of the circular and rectangular texture is thus less asymmetric. This shows that converging micro-textures, such as the modified chevron micro-texture, are superior to non-converging textures in generating an asymmetric pressure distribution where the positive pressure area is larger than that of the negative pressure, due to the wedge effect and squeezing of the fluid, and are recommended when the sliding direction is unidirectional.

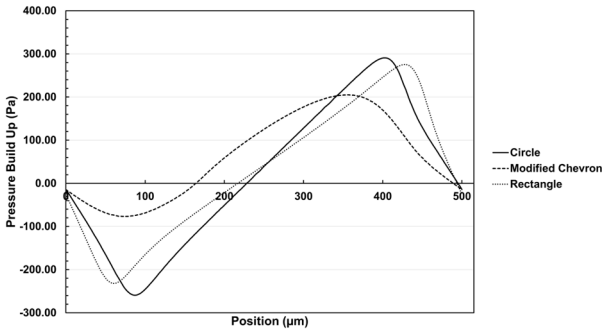


Fig. 17. Pressure build-up curve over the line coincident with section A on the upper sliding surface for the circular and rectangular micro- textures.

TABLE VI. PRESSURE BUILD-UP AND COF RESULTS OF THE RECTANGULAR, CIRCULAR, AND MODIFIED CHEVRON MICRO TEXTURES

| Micro-Texture | Pressure Build-Up (Pa) | COF |
|---|---|---|
| Circle | 19.37 | 4.35 |
| Rectangle | 27.00 | 3.1 |
| Modified Chevron | 38.90 | 2.25 |

## V. EXPERIMENTAL RESULTS

The laser optimization process discussed in Section III.C was essential in order to obtain an accurate and precise geometry for the engraved micro-textures. The rectangular and modified chevron micro-textures were engraved on the surface of the carbide samples, as shown in Fig. 18(a) and (b), respectively, using the femtosecond laser. The laser optimization process consisted of obtaining straight and well-defined edges by setting optimal values for the marking speed and the jumping speed of the laser, while also avoiding focused laser spots at the end or beginning of hatching lines by optimizing the laser on and off delays. The distance between the hatching or engraving lines was also important as it dictated the consistency of the surface inside of the texture, where a small enough distance between the engraved lines was needed for a consistent engraved surface. The rectangle and modified chevron micro-textures were tested under lubricated friction, as well as a non-textured surface.

The untextured surface led to a friction coefficient of 0.1275, while the rectangular texture led to a friction coefficient of 0.1273. The friction reduction is very minimal. These results are expected, as it can be observed from the CFD simulations, that the rectangle micro-texture provides little benefit in increasing hydrodynamic pressure, as it leads to a nearly symmetric pressure distribution. The rectangle's behavior of leading to a low hydrodynamic pressure generation, and thus low benefits or changes in friction is also supported by previous Ref. [28], as converging-shaped textures, such as the chevron texture, can lead to higher pressure generation due to the wedge effect and the squeezing of the fluid inside of the micro-texture. The experimental friction results of the rectangular micro-texture reinforce the CFD results, as it was expected from the rectangular micro-texture to provide minimal benefits in reducing friction due to the low hydrodynamic pressure it generated. On the other hand, the modified chevron micro-texture achieved a friction coefficient of 0.1157, corresponding to a 9.25% decrease relative to the untextured surface and a 9.11% reduction relative to the rectangular micro-texture. This improved friction performance aligns with the larger net-positive pressure build-up observed in the numerical simulations for the modified chevron relative to the rectangular texture. The higher pressure built-up by the modified chevron can be associated with its narrowing geometry along the sliding direction, where a pressure gradient develops due to the wedge effect and mass conversion, thereby producing a local pressure rise and enhanced load support. In contrast, the rectangular micro-texture does not include a converging path and thus exhibits a weaker hydrodynamic pressure build-up.

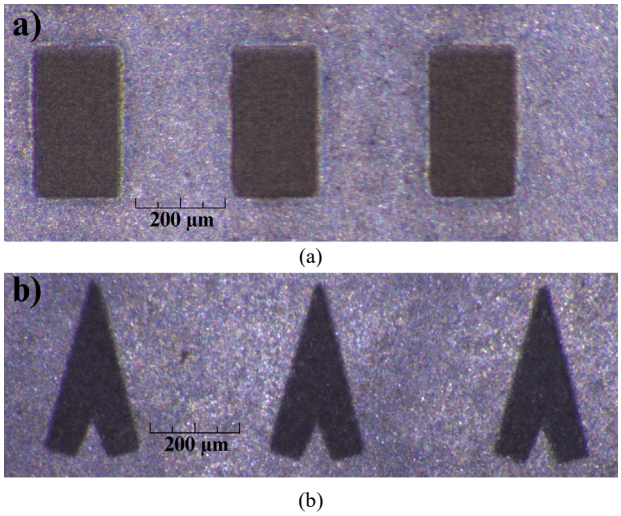


(a)

(b)

Fig. 18. Microscopic pictures of (a) rectangle micro-textured carbide surface and (b) modified chevron micro-textured carbide surface.

## VI. CONCLUSION

The study used CFD simulations in order to better understand how the different geometrical parameters of the chevron micro-texture affect fluid behavior and hydrodynamic pressure, while also proposing a new modified version of the chevron micro-texture. The modified chevron micro-texture with a high leg-width ratio featured a larger outlet converging area, which led to an asymmetric pressure distribution, leading to a net-positive average hydrodynamic pressure build-up, in contrast to the circle and rectangular geometries, who both led to a nearly symmetric pressure distribution due to their non-converging shapes. Experimentally, the modified chevron and rectangular micro-textures were engraved on a carbide surface using a femtosecond laser, and their frictional performance was evaluated. The rectangular micro-texture led to an expected friction reduction performance, as it provided minimal benefits, while the modified chevron micro-texture decreased the friction coefficient by 9.11% compared to the rectangular texture, due to its converging geometry and thus generating a higher net-positive hydrodynamic pressure, as shown by the numerical simulation results. The results of this study provide additional information with regards to the effect of the geometrical parameters of the chevron micro-texture on the fluid behavior, the effect of a newly defined chevron parameter, the leg width ratio, on the hydrodynamic pressure, while also understanding how different micro-texture shapes behave under lubricated friction.

## CONFLICT OF INTEREST

The authors declare no conflict of interest.

## AUTHOR CONTRIBUTIONS

MC and RB contributed to the conception and design of the study, methodology development, software, validation, formal analysis, investigation, resources, and visualization. RB also supervised the study. The first draft

of the manuscript was written by MC, and RB contributed to the review and editing of the manuscript. Both authors commented on previous versions of the manuscript; all authors had approved the final version.

## REFERENCES


[1] B. Mao, A. Siddaiah, Y. Liao *et al.,* "Laser surface texturing and related techniques for enhancing tribological performance of engineering materials: A review," *Journal of Manufacturing Processes,* vol. 53, pp. 153–173, 2020. https://doi.org/10.1016/j.jmapro.2020.02.009

[2] M. S. Brown and C. B. Arnold, "Fundamentals of laser-material interaction and application to multiscale surface modification," in *Laser Precision Microfabrication*, K. Sugioka, M. Meunier, and A. Piqué Eds. Berlin, Heidelberg: Springer Berlin Heidelberg, 2010, pp. 91–120.

[3] Z. Lin and M. Hong, "Femtosecond laser precision engineering: From micron, submicron, to nanoscale," *Ultrafast Science,* 2021. doi: 10.34133/2021/9783514

[4] H. Yin, X. Zhang, Z. Guo *et al.,* "Synergetic effects of surface textures with modified copper nanoparticles lubricant additives on the tribological properties of cylinder liner-piston ring," *Tribology International,* vol. 178, 108085, 2023. https://doi.org/10.1016/j.triboint.2022.108085

[5] L. F. dos Anjos, A. P. Jaramillo, G. C. Buscaglia *et al.,* "Improving the load capacity of journal bearings with chevron textures on the shaft surface," *Tribology International,* vol. 185, 108561, 2023. https://doi.org/10.1016/j.triboint.2023.108561

[6] S. K. Mishra, S. Ghosh, and S. Aravindan, "Characterization and machining performance of laser-textured chevron shaped tools coated with AlTiN and AlCrN coatings," *Surface and Coatings Technology,* vol. 334, pp. 344–356, 2018. https://doi.org/10.1016/j.surfcoat.2017.11.061

[7] R. Long, J. Hou, Y. Zhang *et al.*, "From experimentation to optimization: Surface micro-texturing for low-friction and durable PTFE–steel interfaces under full film lubrication," *Polymers,* vol. 16, no. 24, 3505, 2024. https://www.mdpi.com/2073-4360/16/24/3505

[8] W. Liu, H. Ni, H. Chen *et al.*, "Numerical simulation and experimental investigation on tribological performance of micro-dimples textured surface under hydrodynamic lubrication," *International Journal of Mechanical Sciences,* vol. 163, 105095, 2019. https://doi.org/10.1016/j.ijmecsci.2019.105095

[9] F. Sahlin , S. B. Glavatskih , T. Almqvist *et al.*, "Two-dimensional CFD-analysis of micro-patterned surfaces in hydrodynamic lubrication," *Journal of Tribology,* vol. 127, no. 1, pp. 96–102, 2005. doi: 10.1115/1.1828067

[10] H. Wang, N. Lin, S. Yuan *et al.*, "Numerical simulation on hydrodynamic lubrication performance of bionic multi-scale composite textures inspired by surface patterns of subcrenata and clam shells," *Tribology International,* vol. 181, 108335, 2023. https://doi.org/10.1016/j.triboint.2023.108335

[11] Y. Wei, H. Yan, S. Li *et al.*, "Numerical and experimental study of a sector-shaped surface texture in friction reduction," *Tribology Letters,* vol. 72, no. 2, 60, 2024. doi: 10.1007/s11249-024-01863-3

[12] P. Chen, K. Jin, X. Liu *et al.*, "Tribological performance of textured 316L stainless steel prepared by selective laser melting," *Journal of Materials Engineering and Performance,* vol. 34, no. 1, pp. 461–472, 2025. 10.1007/s11665-023-09009-7

[13] L. Dan, Y. Xuefeng, L. Chongyang *et al.*, "Tribological characteristics of a cemented carbide friction surface with chevron pattern micro-texture based on different texture density," *Tribology International,* vol. 142, 106016, 2020. https://doi.org/10.1016/j.triboint.2019.106016

[14] Z. Shen, F. Wang, Z. Chen *et al*., "Numerical simulation of lubrication performance on chevron textured surface under hydrodynamic lubrication," *Tribology International,* vol. 154, 106704, 2021. https://doi.org/10.1016/j.triboint.2020.106704

[15] N. Zhang, Z. Li, S. Jiang *et al*., "Investigation on tribological performance of lubricating film with chevron texture," *Tribology Transactions,* vol. 66, no. 1, pp. 8–22, 2023. doi: 10.1080/10402004.2022.2130120

[16] G. Schnell, T. Müller, and H. Seitz, "Tribological effects of different scaled chevron-shaped microstructures on the Stribeck curve of parallel contacts under unidirectional friction," *Tribology International,* vol. 178, 108099, 2023. https://doi.org/10.1016/j.triboint.2022.108099

[17] H. L. Costa and I. M. Hutchings, "Hydrodynamic lubrication of textured steel surfaces under reciprocating sliding conditions," *Tribology International,* vol. 40, no. 8, pp. 1227–1238, 2007. https://doi.org/10.1016/j.triboint.2007.01.014

[18] P. Li, F. Zhang, H. Zhang *et al*., "Lubrication performance of kite-shaped microtexture under hydrodynamic lubrication," *Tribology International,* vol. 179, 108144, 2023. https://doi.org/10.1016/j.triboint.2022.108144

[19] H. Yin, J. Yang, and Q. Gu, "Numerical study on the hydrodynamic lubrication performance improvement of bio-inspired peregrine falcon wing-shaped microtexture," *Tribology International,* vol. 191, 109049, 2024. https://doi.org/10.1016/j.triboint.2023.109049

[20] B. Su, X. Zou, Z. Wang *et al*., "Numerical analysis of lubrication properties on a bio-inspired parabolic textured surface," *Meccanica,* vol. 59, no. 6, pp. 987–1000, 2024. doi: 10.1007/s11012-024-01838-7

[21] M. Abhilash, P. Ramkumar, and S. Vengadesan, "Evaluation of tribological performance in contact pairs by implementing the biomimetic surface textures with lubricant flow using CFD techniques," *Industrial Lubrication and Tribology,* vol. 76, no. 5, pp. 639–648, 2024. doi: 10.1108/ILT-02-2024-0053

[22] L. Chen, L. Shang, Z. Liu *et al*., "Effects of chevron micro-textures on tribological and lubricating performance of cylinder block/valve plate interface in axial piston pumps," *Journal of Tribology*, vol. 145, no. 3, 032201, 2022. doi: 10.1115/1.4055302

[23] Z. Kang, Y. Fu, J. Ji *et al.,* "Numerical investigation of microtexture cutting tool on hydrodynamic lubrication," *Journal of Tribology-transactions of The Asme,* vol. 139, 54502, 2017. doi: 10.1115/1.4035506

[24] K. Li, D. Jing, J. Hu *et al.,* "Numerical investigation of the tribological performance of micro-dimple textured surfaces under hydrodynamic lubrication," *Beilstein Journal of Nanotechnology,* vol. 8, pp. 2324–2338, 2017. doi: 10.3762/bjnano.8.232

[25] Q. Allen and B. Raeymaekers, "Soft EHL simulations of lubricant film thickness in textured hard-on-soft bearings considering different cavitation models, in the context of prosthetic hip implants," *Tribology Letters,* vol. 69, no. 4, 118, 2021. doi: 10.1007/s11249-021-01498-8

[26] D. Gropper, L. Wang, and T. J. Harvey, "Hydrodynamic lubrication of textured surfaces: A review of modeling techniques and key findings," *Tribology International,* vol. 94, pp. 509–529, 2016. https://doi.org/10.1016/j.triboint.2015.10.009

[27] R. Bejjani and A. H. Al Fleety, "Investigating the tribological properties under severe contact conditions using an extreme pressure tribo-device," *The International Journal of Advanced Manufacturing Technology,* vol. 135, no. 9, pp. 4731–4748, 2024. doi: 10.1007/s00170-024-14787-y

[28] P. Lu, R. J. K. Wood, M. G. Gee *et al.,* "A novel surface texture shape for directional friction control," *Tribology Letters,* vol. 66, no. 1, 51, 2018. doi: 10.1007/s11249-018-0995-0